Modeling Heterogeneous Downward Dense Gas-Particle Flows

Regis Andreux
CNRS, Laboratoire de Génie Chimique, U.M.R 5503, 05 rue Paulin Talabot, 31106 Toulouse, France

Mehrdji Hémati
ENSIACET, Laboratoire de Génie Chimique, U.M.R 5503, 05 rue Paulin Talabot, 31106 Toulouse, France

DOI 10.1002/aic.12049
Published online October 22, 2009 in Wiley InterScience (www.interscience.wiley.com).

A novel approach is proposed to model heterogeneous downward dense gas-particle flows. The homogeneous behavior of the flow is described by the mass and momentum transport equations of the gas and particulate phases solved using a mono-dimension finite volume method on staggered grids. The heterogeneous features of the flow are predicted simultaneously using the bubble-emulsion formalism. The gas compressibility is taken into consideration. The model is supplemented with a new correlation to account for the wall-particle frictional effects. The predictions are compared with the vertical profiles of pressure and the amount of gas that flows up and down two standpipes and a cyclone dipleg of an industrial fluid catalytic cracking unit and of a cold small-scale circulating fluidized bed. The trends are well predicted. The model gives further information and is thus an innovative starting point for downward dense gas-particle flow hydrodynamics investigation. © 2009 American Institute of Chemical Engineers *AIChE J,* 56: 1163–1172, 2010

Keywords: cyclone, dipleg, standpipe, wall friction, fluidization, modeling

Introduction

Downward dense transport of particles through vertical pipes is a major issue in the fluid catalytic cracking (FCC) process, which converts large quantities of heavy liquid oils to lighter and more valuable gas products. The dense transport can best be achieved while maintaining the particles in a moderately aerated state with interstitial gas. The aerated gas-particle suspension acts as a fluid, and an increase in pressure along the vertical pipe is thus observed. The static pressure head is directly related to the apparent density of the suspension and the height of the pipe.

Standpipe and cyclone dipleg flows are typical examples of such flows. Cyclone diplegs must have constant static pressure head to avoid intermittent gas reversals that will disturb the dipleg flow and modify the particle collection efficiency. Standpipes must have constant high static pressure head to ensure hydraulic oil-tightness between the riser oil cracking zone and the regenerator coke combustion zone and to ensure continuous feeding of catalyst particles: bad control of the FCC unit, flow reversal risks, and emergency shut-down will therefore be avoided.[1]

The interstitial gas is compressed along the vertical pipe because the pressure increases. Consequently, the suspension porosity decreases leading to static pressure head change. When the gas compression exceeds a critical value, the suspension deaerates: particles are compacting, inducing zero static pressure head and particle flow blocking. In the case of cyclones, accurate designs in terms of size and seal height avoid deaeration. In the case of standpipes, external gas injections along the vertical pipe counteract the gas compression effect and maintain the particles in a moderately aerated state. Thus, the pressure and suspension porosity must be well predicted to ensure accurate dense transport. Moreover, the gas that flows up and down the pipe must be anticipated when a hydraulic oil-tightness is required.

Correspondence concerning this article should be addressed to R. Andreux at regis.andreux@ensiacet.fr

Over the years, several models have been proposed to predict the pressure along the vertical flow,[2–7] all essentially stating that the flow is homogeneously fluidized between the minimum fluidizing and bubbling states. The pressure is then estimated using the mathematical expression of the static pressure head and an estimation of the apparent density of the suspension. The gas-particle slip velocity is calculated using the resulting pressure gradient and a classical drag law.[8–10] Finally, the gas velocity is calculated using the slip velocity and the particle velocity that comes from the solid mass flux and the estimated suspension density. When external aerations are employed, the model is supplemented with the gas phase continuity equation to provide the gas velocity along the flow.

Such an approach predicts the vertical profile of pressure and the net gas flow rate. The flow regime can also be anticipated: if the predicted slip velocity is lower that the minimum fluidizing velocity, U_{mf}, the flow pertains to the nonfluidized moving bed regime. If the slip velocity lies between the minimum fluidizing and bubbling velocities, U_{mf} and U_{mb}, the flow belongs to the homogeneous fluidized flow regime. If the slip velocity is higher than the minimum bubbling velocity, U_{mb}, the flow pertains to the heterogeneous fluidized flow regime. However, such an approach cannot be applied when the particle phase weight is not fully carried by the gas phase, i.e., in partially deaerated flow conditions. Indeed, the hydraulic expression of the static pressure head is not valid anymore because of the wall-particle frictional effects. It should not be applied either in heterogeneous flow conditions. Indeed, the usual drag laws of the literature, we previously talked about will provide spurious pressure drops since they are valid only under homogeneous flow conditions. Finally, this approach is not able to predict the contribution of the upward and the downward gas flows to the net gas flow in vertical pipes.

Nowadays, the computational fluid dynamics (CFD) may not be mature enough to pretend to simulate large scale heterogeneous downward dense gas-particle flows. The first limitation resides in the required computational mesh hence the required CPU time to well reproduce the hydrodynamics. Indeed, the heterogeneous structure involves small bubbles of gas whose diameter is below 10 cm. Thus, considering that almost five computational cells are required to describe a structure and its boundaries, the number of cells involved in the representative simulation of an industrial standpipe will be around 2,000,000. High performance of gas-particle parallel codes is thus required to perform the full three-dimension transient simulations. The second limitation lies in the validation of the theory of granular media applied to dense flows of Geldart-A particles. Many papers have reported its inadequacy in simulating these flows, and the most reported cause is the drag modification due to interparticle adhesion forces. Pragmatic fitting of the drag law was then proposed[11,12] but the direct transposition to downward dense heterogeneous flows without preliminary validations is highly questionable. Finally, the simulations will be highly unstable because the numerical management of compacting particles is a very tough process.[13]

As a conclusion, it seems that none of the models that have been proposed in the literature are today able to predict the heterogeneous downward dense gas-particle flows.

The objective of this article is to give a model that is capable of predicting the heterogeneous downward dense gas-particle flow behaviors with acceptable CPU time requirement. The model combines the Eulerian two-fluid formalism that is usually used in gas-particle CFD and the bubble-emulsion formalism that is generally used in the chemical engineering field. The model is mono-dimensional. We show that such an approach is able to describe the heterogeneous structure of the flow without tremendous computational meshes which usually lead to heavy simulations with prohibitive CPU Time.

We will first describe the equations and then benchmark the model. Three test cases are considered:

- the standpipe of an industrial FCC unit;
- the standpipe of a cold small-scale circulating fluidized bed (CFB);
- the cyclone dipleg flows of a cold small-scale CFB.

Description of the Model

The illustration of the formalism is shown in Figure 1. The first fluid is the gas phase that consists of the bubble and emulsion gas phases; the second is the particles that flow down the vertical pipe. Separate Eulerian conservation equations are formulated for the mass and momentum balance of the overall gas and particle phases coupled through interfacial momentum transfer terms due to drag. As a first approximation, we assume that the momentum transfer between the interstitial gas of the emulsion and the solids is the dominant contribution to the drag force. The bubble phase is thus not involved in the drag force calculation. The bubble and emulsion phases are described using the classical fluidized bed reactor model approach supplemented with an expression that correlates the local fluidizing velocity to the local suspension porosity dedicated to FCC powders. Gas compressibility is accounted for and is assumed to be the same as an ideal gas. The resulting set of equations is solved by a finite volume method on staggered grids.

Overall gas mass balance equation

$$\frac{\partial \rho_g \varepsilon U_g}{\partial x} = S_g, \tag{1}$$

where ρ_g is the density of the overall gas, ε the gas volumetric concentration of the suspension, U_g the interstitial velocity of the overall gas, and S_g is the gas source term related to the external gas aerations.

Particle mass balance equation

$$\frac{\partial \rho_p \varepsilon_p U_p}{\partial x} = 0, \tag{2}$$

where ρ_p is the density of the particles, $\varepsilon_p = 1 - \varepsilon$ is the particle volumetric concentration of the suspension, and U_p is the interstitial velocity of the particles.

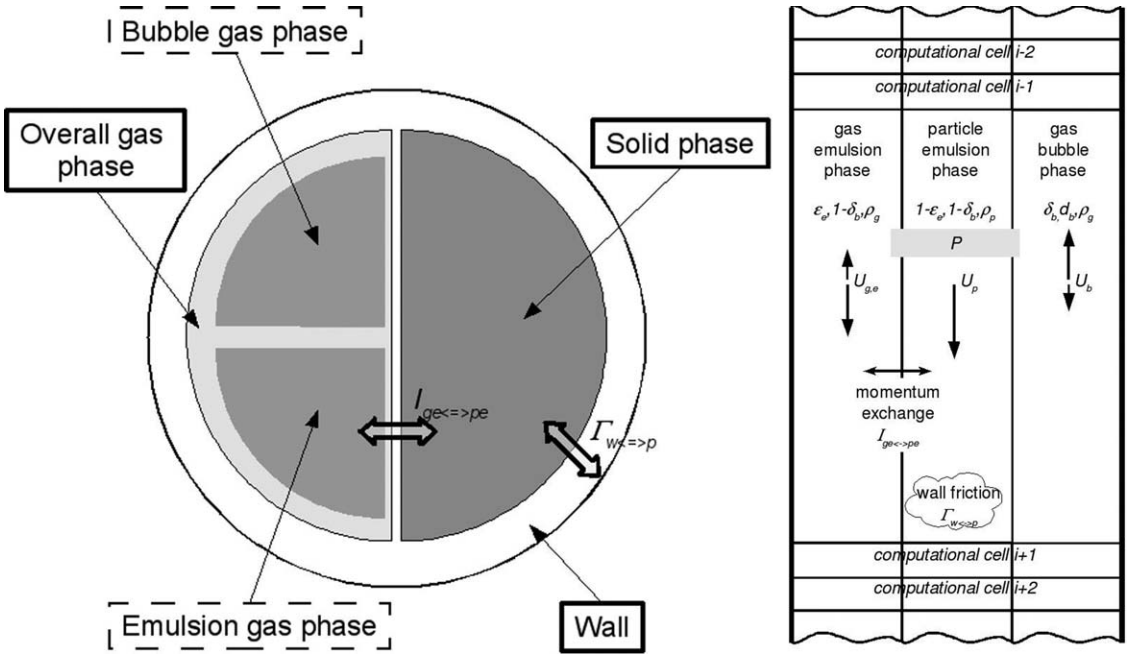

Figure 1. Illustration of the formalism of the heterogeneous downward dense gas-particle flow modeling.

Gas momentum balance equation

$$\frac{\partial \rho_g \varepsilon U_g U_g}{\partial x} = -\varepsilon \frac{\partial P}{\partial x} + \varepsilon \rho_g g + I_{ge \Leftrightarrow pe}, \tag{3}$$

where P is the mean pressure of the gas phase, and $I_{ge \Leftrightarrow pe}$ is the interfacial momentum transfer term between the gas and particles in the emulsion phase.

Particle momentum balance equation

$$\frac{\partial \rho_p \varepsilon_p U_p U_p}{\partial x} = -\varepsilon_p \frac{\partial P}{\partial x} + \varepsilon_p \rho_p g - I_{ge \Leftrightarrow pe} - \Gamma_{w \Leftrightarrow p}, \tag{4}$$

where $\Gamma_{w \Leftrightarrow p}$ is the wall-particle frictional force. This term will be further discussed in the section dedicated to the simulation results.

Bubble-emulsion modeling

As a first approximation, the bubbles are assumed to be free of particles and the emulsion porosity equals the minimum bubbling porosity ($\varepsilon_e = \varepsilon_{mb}$). Therefore, the local gas mass balance is ensured by the following relation, which is used to calculate the volumetric fraction of the emulsion phase, δ_e:

$$\varepsilon = (1 - \delta_e) + \delta_e \varepsilon_{mb}. \tag{5}$$

The velocity of the emulsion gas phase is calculated solving the corresponding momentum balance equation:

$$\frac{\partial \rho_g \delta_e \varepsilon_{mb} U_{g,e} U_{g,e}}{\partial x} = -\delta_e \varepsilon_{mb} \frac{\partial P}{\partial x} + \delta_e \varepsilon_{mb} \rho_g g + I_{ge \Leftrightarrow pe}. \tag{6}$$

The local bubble velocity, U_b, is calculated using the Davidson-Harrison correlation,[14] relatively to the downward particle velocity U_p:

$$U_b = \left(U_f - \varepsilon_{mb} U_{g,e} + 0.711\sqrt{9.81 d_b}\right) - U_p, \tag{7}$$

where d_b is the average bubble diameter and U_f is the local fluidizing velocity calculated using the Leung-Jones[4] correlation:

$$U_f = 1.36 - 6.66\varepsilon_g + 8.4\varepsilon_g^2. \tag{8}$$

Since the bubble diameter quickly reaches its maximum size in air-FCC fluidized beds,[15] it is considered constant and equals the maximum value reported by Geldart and Radtke[16] and Andreux and Chaouki[17]: $d_b = 6$ cm.

Gas density

The local gas density is calculated assuming ideal gas with a molar mass M:

$$\rho_g = \frac{PM}{RT}, \tag{9}$$

where P is the local pressure, T the local temperature, and R the universal gas constant that equals 8.314 J/(mol K).

Pressure

The pressure–velocity coupling is solved using an iterative process until convergence.

Interfacial momentum transfer between gas and particles of the emulsion phase

The interfacial momentum transfer between gas and particles of the emulsion phase consists of the drag force:

Table 1. Operating Conditions and Data from the Literature for the Model Validation

Reference	G_s (kg/m^2/s)	D (m)	L (m)	Aeration: Total Rate (Nm^3/h)	Aeration: Position	Particles	Reported Data
Srivastava[19]	638	1.155	≈30	2500	(not reported) 10 uniformly distributed taps	Typical FCC	Pressure vertical profiles
Srivastava et al.[20]	345	0.076	≈8	0.326	9 uniformly distributed taps	80 μm, 1700 kg/m^3	
	720			2.775			
	915			3.976			
	1020			5.185			
Karri and Knowlton[21,22]	50-600	0.100	2.5	1.1	1 at the bottom dipleg	76 μm, 1442 kg/m^3	Up and down gas mass fluxes

$$I_{ge\Leftrightarrow pe} = \frac{3}{4}(1-\varepsilon_{mb})\delta_e\rho_g\frac{C_d}{d_p}\left|U_p - U_{g,e}\right|\left(U_p - U_{g,e}\right). \quad (10)$$

Following Wen and Yu,[9] the drag coefficient C_d is calculated as follows:

$$C_d = C_d^s\varepsilon_{mb}^{-1.7} = \left(\frac{24}{Re_p}\left(1+0.15Re_p^{0.687}\right)\right)\varepsilon_{mb}^{-1.7}, \quad (11)$$

where C_d^s is the drag coefficient of a single sphere from Schiller-Nauman,[18] and Re_p the Reynolds particle number defined as:

$$Re_p = \varepsilon_{mb}\rho_g\left|U_p - U_{g,e}\right|d_p/\mu_g. \quad (12)$$

Numerical Methods

Numerical solver

The equations are implemented in C++. Finite volume methods are used on staggered velocity and pressure grids using a segregated approach, in which equations are formulated for each dependent variable and solved sequentially. An iterative process is used to reach the steady-state solution.

Implementation of boundary conditions

The type of boundary condition used for the gas velocity equation is a zero gradient, namely:

$$\frac{\partial U_g}{\partial x} = 0, \quad (13)$$

for all boundaries where the pressure is specified. The top boundary condition for the pressure equation is a fixed value the user is asked for at the beginning of the simulation. The bottom boundary condition for the pressure equation is a fixed value set by the user or is calculated by the code as the total static pressure head after subtracting the total wall-particle friction force along the vertical pipe:

$$P_{bottom} = \int_0^H \left[(1-\varepsilon(x))\rho_p g - \Gamma_{w\Leftrightarrow p}(x)\right]dx \quad (14)$$

The type of boundary condition used for the particle velocity equation is a fixed value at the top and a zero gradient at the bottom. Similar boundary conditions are likewise considered for the particle mass balance equation.

Computational domain

The vertical flow is discretized into N computational cells of 10 mm high.

Description of the Test Cases

The model ought to be benchmarked using experimental data that provide information about pressure gradients, solid volumetric concentrations, velocities and volumetric fractions of the bubble phase, and amounts of gas traveling upward and downward. Experimental information about the effects of the pipe dimensions, external aeration rates and positions, and top and bottom pressure should also be used.

However, such exhaustive work has never been reported in the literature. Thus, the partial validation of the model is performed comparing its predictions to available measurements that are representative of the field of our interest:

- the vertical profile of the pressure along the standpipe of a Fluid Catalytic Cracking Unit,
- the vertical profiles of the pressure along the standpipe of a cold small-scale CFB,
- the amount of gas that travels upward and downward through the dipleg of a cyclone.

The industrial FCC standpipe

The operating conditions are summarized in Table 1. The industrial data are reported by Matsen.[19] The catalyst is flowing downward in an industrial standpipe 1155 mm in diameter and 30 m high. The catalyst circulation rate is equal to 40 t/min, which is equivalent to a solid mass flux of 638 kg/m^2/s. The particles are typical FCC catalysts with a minimum fluidizing velocity of 1.5 mm/s. Since no more particle information is provided, we assumed that the density is equal to 1550 kg/m^3 to calculate the average particle size diameter using the correlation of Wen and Yu: 55 μm. The top and bottom pressures are equal to 1.875 and 3.254 bars, respectively. The operating temperature is equal to 607°C, which is questionable since it is a very low value for an FCC regenerator (however, we consider this value in our simulation). The total aeration rate is equal to 2500 Nm^3/h. Tap locations are not specified, and we then consider 10 uniformly distributed taps.

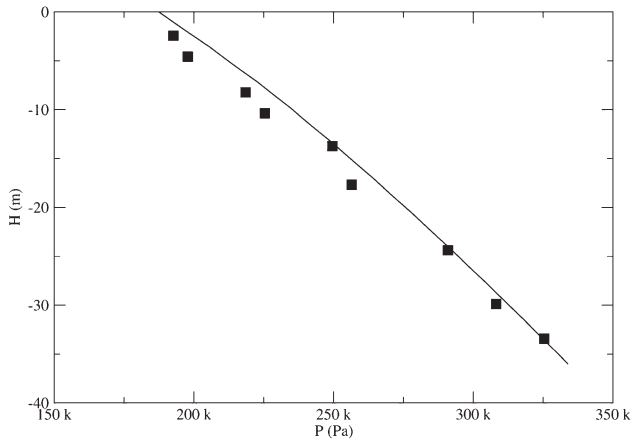

Figure 2. Comparison between the vertical profile of pressure predicted by the model (—) and the industrial data of Matsen[19] (■).

The cold small-scale CFB

The operating conditions are summarized in Table 1. The cold small-scale CFB is the one of Srivastava et al.[20] It consists of a 7.6-m high, 76-mm diameter Plexiglass standpipe fed from a fluidized bed. The catalyst circulation and external aeration rates are equal to 345 kg/m^2/s and 0.326 Nm^3/h, 720 kg/m^2/s and 2.775 Nm^3/h, 915 kg/m^2/s and 3.976 Nm^3/h, and 1020 kg/m^2/s and 5.185 Nm^3/h, respectively. The particles are typical FCC catalysts with a density of 1700 kg/m^3, and an average diameter of 80 μm. The top pressure is equal to 1.070 bars. Experiments are performed at room temperature. Nine aeration taps are used distributed uniformly along the standpipe.

The cyclone dipleg flow

The cyclone dipleg is the one of Karri and Knowlton.[21,22] It is 100 mm in diameter and 2.5 m high. The catalyst mass flux through the dipleg ranges between 50 and 600 kg/m^2/s. The particles are typical FCC catalysts with a density of 1442/m^3 and an average diameter of 76 μm. The dipleg pressure drop is kept constant and is equal to 4300 Pa. The inlet conditions cannot be easily identified: the particles slide down the periphery of the cyclone barrel and cone, and then enter the dipleg so that it is quite impossible to specify uniform inlet profiles of the volumetric concentration and velocity. Thus, the inlet solid concentration is arbitrarily set at 0.3, which can be considered as the beginning of the dense regime. The inlet solid velocity is then adjusted to obtain the required solid mass flux. As in the experiments, a small amount of aeration at the bottom of the dipleg is added (1.1 Nm^3/h).

Results and Discussion

Although the cases considered here are not really simple, the computations clearly show that no spurious field occurs either in the pressure or in the velocity fields. Moreover, the computations report overwhelmingly significant reduction in the required CPU time to achieve a converged steady-state flow compared with the CFD approach: $\sim$1 CPU minute. Hence, the model and the numerical method we propose fulfill the requirements to be an innovative tool for dense gas-particle downward flow hydrodynamics investigation.

The industrial FCC standpipe

The vertical profile of the pressure, P, is well predicted even when the wall-particle frictional effect is not counted (Figure 2). It confirms Matsen's approximation which states that the wall-particle frictional effect is negligible. In such conditions, the apparent density of the flowing mixture calculated with the pressure gradient value equals the actual density.

Matsen observed that the pressure profile slope is higher in the top half of the vertical profile than in the bottom half. The model reproduces this trend. The computation shows that when gas is injected in the standpipe to maintain the particles in an aerated state, it enters directly into the bubble phase and affects the local porosity of the suspension, ε, in a similar manner and so the apparent density (Figure 3). Indeed, the volumetric fraction of the bubble phase, δ_b, increases suddenly at the elevation of each aeration tap while it decreases regularly below because of the pressure going up. Likewise, the suspension porosity, ε. Therefore, the decrease in the pressure profile slope should be explained by the effect of aeration that overcounteracts the gas compression and induces a regular increase in the suspension porosity down the standpipe. Note that following the definition of Leung and Jones,[2,23] the flow pertains to the dense phase fluidized flow regime since the local suspension porosity increases below the aeration taps. The standpipe is slightly over-aerated.

The model also predicts that the downward gas flow rate through the bubble phase, $\delta_b \varepsilon_b \rho_g U_i$, suddenly increases at the elevation of each aeration tap in a similar manner (Figure 4). The gas flow rate through the emulsion phase, $\delta_e \varepsilon_{mb} \rho_g U_{g,e}$, is not affected by the external aeration. In other words, the region around each aeration tap is a stiff

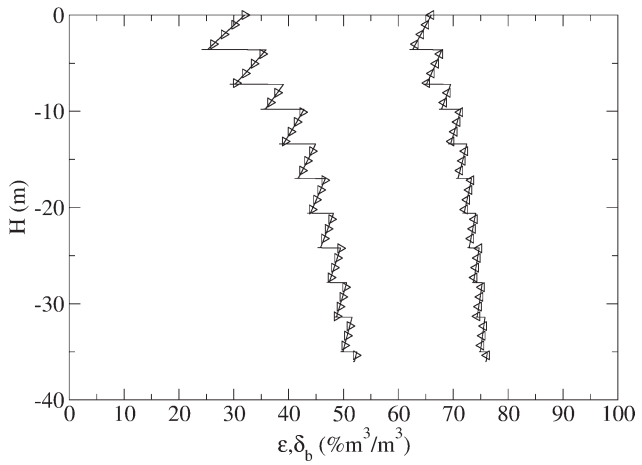

Figure 3. Model prediction of the industrial standpipe reported by Matsen[19]: local bubble phase fraction, δ_b (▷) and local suspension porosity, ε (◁).

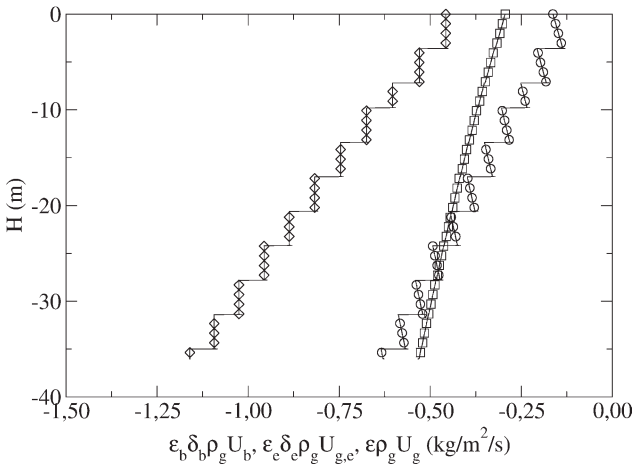

Figure 4. Model prediction of the industrial standpipe reported by Matsen[19]: local gas mass flux through the bubble phase, $\delta_b \varepsilon_b \rho_g U_b$ (○), the emulsion phase, $\delta_e \varepsilon_e \rho_g U_{g,e}$ (□), and total value, $\varepsilon \rho_g U_g$ (◇).

transition zone between relatively smooth and "shaken" hydrodynamics with strong shear and high solid mixing. From the industrial point of view, this could lead to local erosion damages and particle attrition.

The computations show that a decrease in the aeration rate reduces the strong variation in the bubble phase volumetric fraction and gas flux, δ_b and $\delta_b \varepsilon_b \rho_g U_b$, at the elevation of each aeration (Figures 5 and 6). Consequently, the transition is less stiff. The amount of bubbles in the standpipe decreases, leading to flow stability improvement since bubbles are known to play a significant role on the downward particle flow disturbance.[24–26] Moreover, the suspension porosity, ε, decreases leading to an increase in the pressure profile slope (Figure 7).

The computation shows that upward gas flow never occurs. It thus confirms the existence of a hydraulic oil-tightness between the riser oil cracking zone and the regenerator coke combustion zone.

The computations confirm that a modification in the behavior of the dense fluidized bed from which the suspension is withdrawn has a great effect on the standpipe operation (Figure 8). When the fluidizing velocity of the upstream fluidized bed is reduced (the consequent top porosity is equal to 57%), the pressure at the bottom of the standpipe increases. However, a high amount of gas should be injected to prevent particle compaction. The main consequence is an increase of the stiff transition at the elevation of each injection. On the contrary, particle withdrawing from a highly turbulent fluidized bed with a porosity of 85% reduces the stiff transitions but also decreases the standpipe bottom pressure, which one should avoid when operating an FCC Unit.

The cold small-scale CFB

The slope of the pressure profile is highly overestimated when the wall-particle frictional effect is not counted (Figure 9). The reason is that the experimental particle weight is not fully supported by the drag force produced by the gas because of the wall-particle frictional forces, particularly at low solid mass fluxes. Thus, the wall-particle frictional effects must be accounted for in the simulations. In an attempt to reproduce the experimental data, modeling aspects of wall-particle frictional effects using hydraulic analogy are discussed.

In single-phase flows, the wall-fluid friction term $\Gamma_{w \leftrightarrow fluid}$, is calculated as:

$$\Gamma_{w \Leftrightarrow fluid} = \lambda \frac{\rho_{fluid} U_{fluid}^2}{2 D_{pipe}}, \tag{15}$$

where ρ_{fluid} and U_{fluid} are the density and the superficial velocity of the fluid, respectively. λ is the pressure drop coefficient, given by:

$$\lambda = a Re_{fluid}^b, \tag{16}$$

where Re_{fluid} is the Reynolds number of the fluid, a and b are constants (for example, $a = 64$ and $b = -1$ in laminar fluid flows).

Therefore, the equivalent expression of the wall-particle friction model dedicated to dense gas-particle suspension flows is:

$$\Gamma_{w \Leftrightarrow p} = \lambda \frac{\rho_{susp} U_{susp}^2}{2 D_{pipe}} = \left[a \left(\frac{\rho_{susp} U_{susp} D_{pipe}}{\mu_{susp}} \right)^b \right] \frac{\rho_{susp} U_{susp}^2}{2 D_{pipe}} \tag{17}$$

where $\rho_{susp} = \varepsilon_g \rho_g + (1 - \varepsilon_g) \rho_p$ is the actual density of the suspension, U_{susp} is taken equal to the downward particle velocity U_p, and μ_{susp} is the apparent viscosity of the gas-particle suspension calculated from the proposal of Thomas[27]:

$$\mu_{susp} = \mu_g (1 + 2.5(1 - \varepsilon_{mb}) + 10.05(1 - \varepsilon_{mb})^2 + 0.00273 e^{16.6(1 - \varepsilon_{emb})} \tag{18}$$

Our wall-particle frictional model differs from the correlations reported in the literature in that it involves the apparent

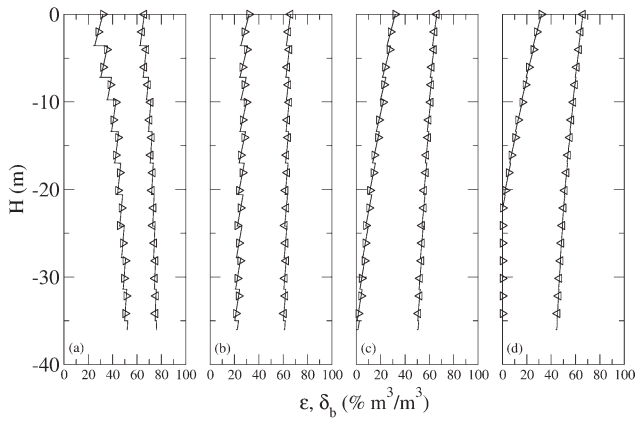

Figure 5. Effect of the aeration rate on the local suspension porosity, ε (◁), and the local bubble phase fraction, δ_b (▷).

Application to Matsen's industrial standpipe in over-aerated conditions (a), well-aerated conditions (b), slightly under-aerated conditions (c), and highly under-aerated conditions (d).

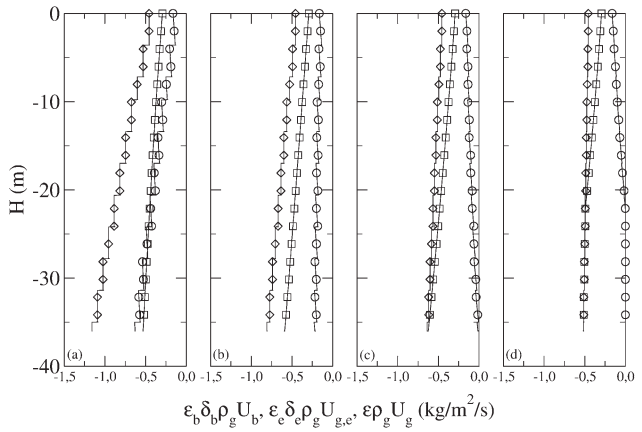

Figure 6. Effect of the aeration rate on the gas mass flux through the bubble phase, $\delta_b\varepsilon_b\rho_g U_b$ (○), the emulsion phase, $\delta_e\varepsilon_e\rho_g U_{g,e}$ (□), and total value, $\varepsilon\rho_g U_g$ (◇).

Application to Matsen's industrial standpipe in over-aerated conditions (a), well-aerated conditions (b), slightly under-aerated conditions (c), and highly under-aerated conditions (d).

density and viscosity of the gas-particle suspension through its Reynolds number. However, it seems hazardous to compare our proposal with others from the literature because of the difference between the formalisms they are based on:

• The wall-particle friction model of the CFD: CFD solves the balance equations of the gas and particle phases. Thus, wall slip boundary conditions have been proposed for the particle phase and not for the suspension. The conditions of Johnson and Jackson[28] are generally used but the granular pressure must be known. Then, supplementary equations derived from the kinetic theory of granular media should be solved. The comparison between our modeling and the CFD approach would thus require performing the CFD simulations, which is not the purpose of our study.

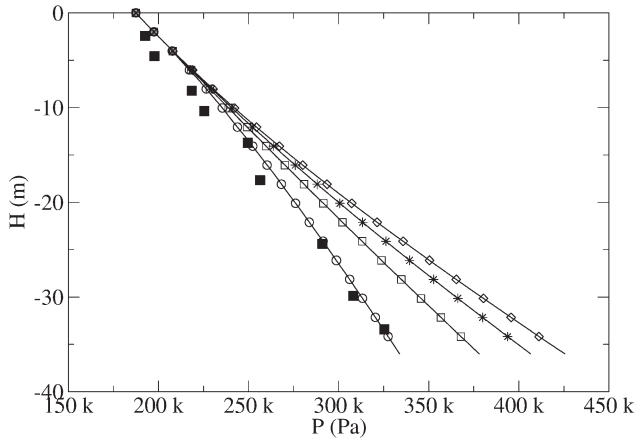

Figure 7. Effect of the aeration rate on the vertical profile of pressure.

Application to Matsen's industrial standpipe in over-aerated conditions (○), well-aerated conditions (□), slightly under-aerated conditions (*), and highly under-aerated conditions (◇).

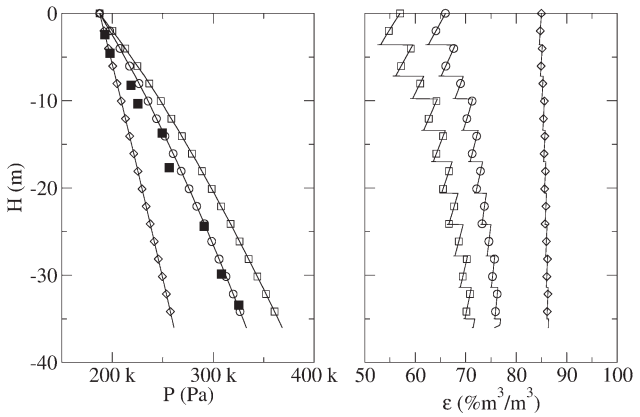

Figure 8. Effect of the inlet condition on the predicted vertical profile of pressure, *P* (left), and local suspension porosity, ε (right), in Matsen's industrial standpipe.

$\varepsilon_{susp,top}$ = 0.57 (◇), $\varepsilon_{susp,top}$ = 0.66 (○), $\varepsilon_{susp,top}$ = 0.85 (□).

• The wall-particle friction model of the mono-dimensional modeling of dilute flows: it usually involves wall-particle frictional laws in terms of the particle velocity only.[29–32] Such formalism does not account for the particle volumetric concentration and is valid only for dilute or semi-dilute gas-particle flows. The transposition of such an approach to the gas-particle dense flow regimes we are interested in is not possible.

On the basis of experimental data, we performed a parameter optimization study to assess the coefficients a and b of (Eq. 16). It leads to the following proposal: $a = 289.5 \times 10^6$, $b = -1.4446$ (Figure 10). The slope of the pressure profiles are now well reproduced over the range of operating conditions (Figure 9). However, the effect of the standpipe's bottom end is still not well reproduced. The main reason is

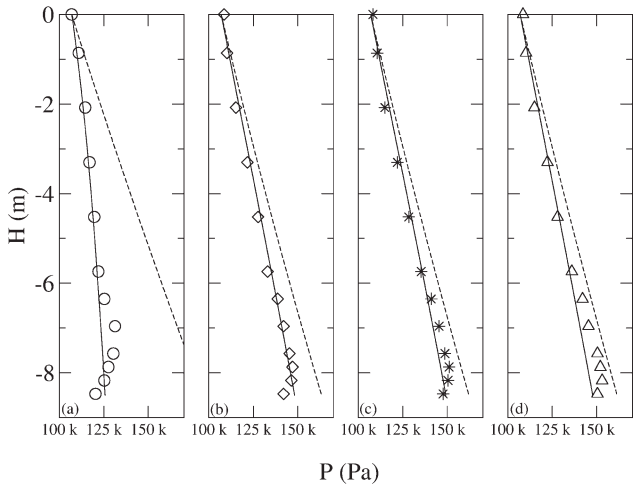

Figure 9. Comparison between the vertical profile of pressure predicted by the model (with friction: —, without friction: ---) and the small-scale moke-up data of Srivastava (symbols).

1.55 kg/s, ---, —, ○; 3.23 kg/s, ---, —, ◇; 4.14 kg/s: ---, —, *; 4.65 kg/s, ---, —, △.

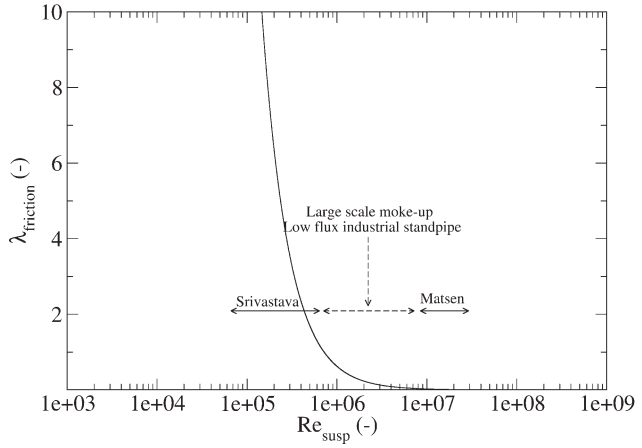

Figure 10. Correlation of the wall-particle frictional effect, based on the measurements assessed on the small scale and industrial standpipes reported by Srivasatava et al.[20] and Masten.[19]

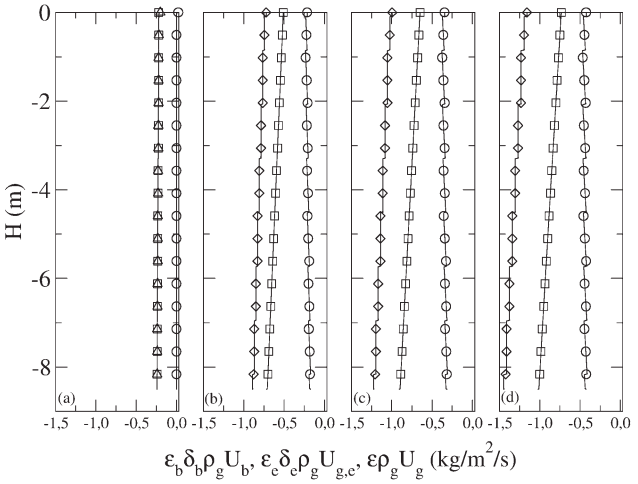

Figure 12. Model prediction of the small-scale standpipe reported by Masten[19]: local gas mass flux through bubble phase, $\delta_b\varepsilon_b\rho_g U_b$ (○), the emulsion phase, $\delta_e\varepsilon_e\rho_g U_{g,e}$ (□), and total value, $\varepsilon\rho_g U_g$ (◇).

that the full physics of the standpipe's bottom end flow are not modeled: reduction in the standpipe section, flow acceleration, high wall effects, and potential coupling with the downstream hydrodynamics, …. Further improvements on the description of the bottom boundary condition are requested.

The computations show that the aerating gas enters directly the bubble phase at the elevation of each aeration tap in a similar manner to the industrial standpipe case (Figure 11). However, the amount of gas that is injected counteracts well the compression effect. Indeed, the decrease in the volume fraction of the gaseous bubble phase, δ_b, between two consecutive aeration taps is more or less equal to the sudden increase observed at the injection location. The total variation in the volumetric fraction of the bubble phase never exceeds 10%: the standpipe flow is well controlled. The good control of the standpipe hydrodynamics is also favored by the low amount of bubbles at the top of the standpipe (nearly half of the industrial case), which induces higher gas mass flow rates through the emulsion phase than through the bubble phase (Figure 12). Following[24–26] the low amount of bubbles in the standpipe is increasing the stability. Following the definition of Leung and Jones,[2,23] the flows pertain to the dense phase fluidized flow regime excepted the 345 kg/m^2/s flow that pertains to the homogeneous moving bed regime for which all the gas travels through the emulsion phase (Figures 11a and 12a).

The computations show that upward gas flow never occurs: it underlines the existence of a hydraulic air-tightness at the bottom of the standpipe.

The cyclone dipleg flow

The predicted net gas flux in the dipleg is presented in Figure 13. The results are plotted on an exact reproduction

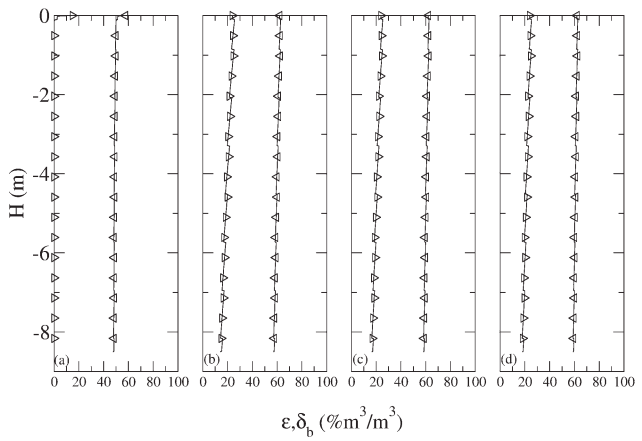

Figure 11. Model prediction of the small-scale standpipe reported by Srivastava et al.[20]: local suspension porosity, ε, (◁) and local fraction of the bubble phase, δ_b, (▷).

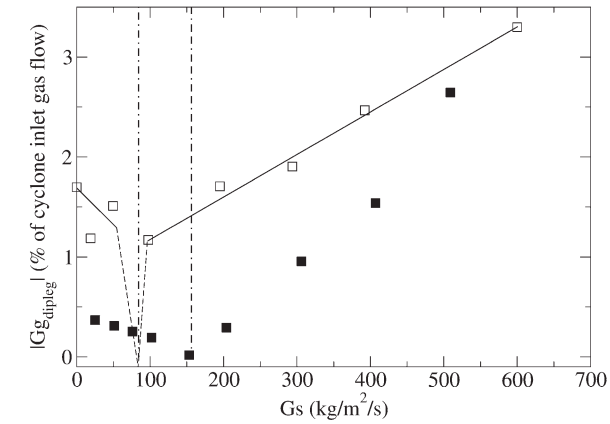

Figure 13. Absolute net gas mass flux through the dipleg made nondimensional by the experimental cyclone inlet gas mass flux of Karri and Knowlton (□, experimental values; ■, predicted values).

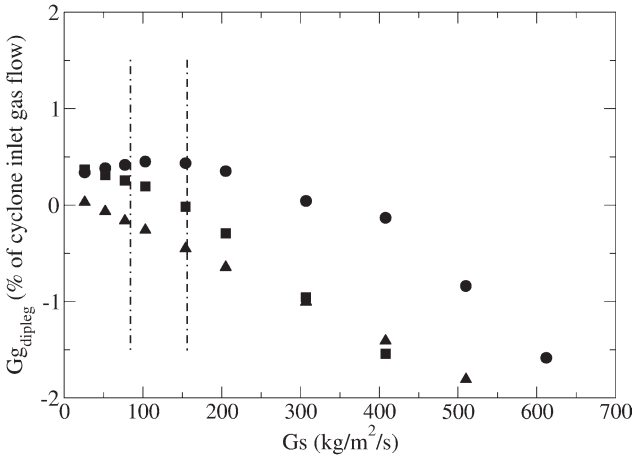

Figure 14. Gas mass flux of the bubble (•) and emulsion (▲) phases and net value (■) through the dipleg made nondimensional by the experimental cyclone inlet gas mass flux of Karri and Knowlton.

of the figure presented by Karri and Knowlton[21] and Knowlton and Karri (2008)[22]. The absolute values are made nondimensional by the experimental inlet gas mass flux of the upstream cyclone, 24 kg/m^2/s. These authors have reported downward average gas flow down the dipleg when the solid mass flux is lower than ~90 kg/m^2/s and upward otherwise. The transition they observed between up and down gas flow regimes is illustrated by the vertical dot-dashed line that divides the set of experimental results (the white squares with linear interpolation curve) into two parts at 90 kg/m^2/s. The transition was not directly observed and their graphical method to calculate the solid mass flux transition point is illustrated by the "V" dashed line centered on 90 kg/m^2/s.

Our computations evidence a solid mass flux transition between the up and down net gas flow regimes, which is ~150 kg/m^2/s. The predicted transition is illustrated on the figure by a vertical dot-dashed line. The predicted trends of the upward and downward net gas flow before and after the transition are linear with slopes comparable to the experimental ones. Karri and Knowlton[21,22] reported a transition solid mass flux lower than ours, approximately of 100 kg/m^2/s. However, the fact that the experimental transition does not correspond to a zero net gas flow relative to the wall is confusing. Furthermore, the method of determination suggests a sudden transition between up and down net gas flow regimes that is not reproduced by our model. These differences may be explained by the trickle valve attached to the experimental dipleg that is not accounted for in the simulations. Further improvements on the description of the bottom boundary conditions are requested.

Figure 14 presents the predicted net, negative, and positive gas mass fluxes through the dipleg depending on the solid mass flux. The experimental and the predicted transition between the downward and the upward gas flow regimes are illustrated by the vertical dot-dashed lines at 90 and 150 kg/m^2/s. At 150 kg/m^2/s, the net gas flow is zero relative to the wall, and the upward and downward gas mass fluxes through the bubble and emulsion phases are equal. When the solid mass flux ranges between 150 and 400 kg/m^2/s, the bubble gas flows up even if the net gas flow in the dipleg is down. In such a condition, the fluid-tightness is thus not perfect. The cyclone dipleg must operate at solid mass fluxes higher than 400 kg/m^2/s to ensure a perfect fluid-tightness. The model clearly underlines that the classical approach consisting in the overall gas flow description must be improved counting individually the bubble and the emulsion gas flow. Otherwise, the operating condition that ensures a perfect fluid-tightness will lacking.

Conclusion

We proposed a novel approach to model the heterogeneous downward dense gas-particle flows. Eulerian–Eulerian gas-particle mass and momentum equations were solved to describe the homogeneous behavior of the flow. The heterogeneous behavior was described using the bubble-emulsion formalism that is commonly used to simulate the dense fluidized beds in the chemical engineering field. The equations were solved using a finite volume method on pressure and velocity staggered grids. Gas compressibility was accounted for.

The model was benchmarked on three cases representative of our field of interest: the standpipe of an FCC unit, the standpipe of a cold small-scale CFB, and a cyclone dipleg. The model was able to reproduce the features of the flows and to give further information:

- the vertical profile of pressure and the effect of the external aerations are well predicted,
- external aeration rate and operating conditions can be improved to increase the standpipe bottom pressure and decrease the potential local erosion damages and particle attrition,
- the existence of the required oil-tightness at the bottom of the industrial standpipe is predicted, specific wall-particle frictional laws can be assessed coupling the model and experiments,
- the amount of gas that flows up and down depending on the operating conditions can be predicted.

The limitations of the present model were underlined. The improvement of the description of the bottom end of the flow is of primary importance.

Notation

g = gravity (m/s^2)
C_d = drag coefficient in the emulsion phase
C_d^s = drag coefficient of a single particle
D = standpipe diameter (m)
d_b = diameter of the bubble phase (m)
g = gravity (m/s^2)
$G_{g,dipleg}$ = gas mass flux in dipleg (kg/m^2/s)
G_s = solid mass flux (kg/m^2/s)
$I_{ge\Leftrightarrow pe}$ = interfacial momentum transfer between gas and particle of the emulsion phase (kg/m^2/s^2)
M = molar mass of the interstitial gas (g/mol)
P = absolute pressure (Pa)
R = universal gas constant (J/mol/K)
Re_p = particle Reynolds number
Re_{susp} = suspension Reynolds number
T = temperature (K)
U_b = velocity of the bubble phase (m/s)

U_f = fluidizing velocity (m)
U_g = interstitial gas velocity (m/s)
$U_{g,e}$ = interstitial gas velocity in the emulsion phase (m/s)
U_{mb} = minimum bubbling porosity of the particles (m/s)
U_{mf} = minimum fluidizing velocity of the particles (m/s)
U_p = downward interstitial particle velocity (m/s)
U_{susp} = superficial velocity of the suspension (m/s)
x = axis position along the vertical pipe (m)

Greek letters

δ_b = volume fraction of the bubble phase (m^3/m^3)
δ_e = volume fraction of the emulsion phase (m^3/m^3)
ε = porosity of the suspension (m^3/m^3)
ε_b = porosity of the bubble phase (m^3/m^3)
ε_e = porosity of the emulsion phase (m^3/m^3)
ε_{mb} = minimum bubbling porosity (m^3/m^3)
ε_{mf} = minimum fluidizing porosity (m^3/m^3)
λ = pressure drop coefficient due to wall friction
μ_g = gas viscosity (Pa.s)
μ_{susp} = apparent viscosity of the gas-particle suspension (Pa.s)
ρ_g = gas density (kg/m^3)
ρ_p = particle density (kg/m^3)
ρ_{susp} = density of the gas-particle suspension (kg/m^3)
$\Gamma_{w\leftrightarrow p}$ = friction force between the wall and the suspension (N/m)
τ_p = wall friction stress (N/m^2)

Literature Cited

1. Mott RW. Troubleshooting FCC standpipe flow problems, *Davidson Catagram*. 1992;83:23–35.
2. Leung LS, Jones PJ. Flow of gas–solid mixtures in stanpipes. A review. *Powder Technol*. 1978;20:145–160.
3. Leung LS, Jones PJ. An analysis of moving-bed flow of solids down standpipes and slide valves. *Powder Technol*. 1978;19:7–15.
4. Leung LS, Jones PJ. Coexistence of fluidized solids flow and packed bed flow in standpipes. In: Davidson JF, Ed. *Proceedings of the International Fluidization Conference*. Cambridge: Cambridge University Press, 1978:116–121.
5. Leung LS. The ups and downs of gas–solid flow—a review. In: Grace JR, Matsen JM, editors. *Fluidization*. New York: Plenum Press, 1980:25–68.
6. Gauthier TA, Ross JL. Controlling gas flow in standpipe systems. In: Werther J, editor. *Proceedings of the 6th International Conference in Circulating Fluidized Beds*, Würsburg, Germany, August 22–27, 1999: 483–489.
7. Bodin S, Briens C, Bergougnou MA, Patureaux T. Standpipe flow modeling, experimental validation and design recommendations. *Powder Technol*. 2002;124:8–17.
8. Ergun S. Fluid flow trough packed columns. *Chem Eng Prog*. 1952;48:89–94.
9. Wen CY, Yu YH. Mechanics of fluidization. *Chem Eng Prog Symp Ser*. 1966;62:100–111.
10. Richardson JF, Zaki WN. Sedimentation and fluidization: Part I. *Trans Instn Chem Eng*. 1954;32:35–53.
11. Jiradilok V, Gidaspow D, Damronglerd S, Koves WJ, Mostofi R. Kinetic theory based CFD simulation of turbulent fluidization of FCC particles in a riser. *Chem Eng Sci*. 2006;61:5544–5559.
12. Sharma SD, Pugsley T, Delatour R. Three-dimensional CFD model of the deaeration rate of FCC particles. *AIChE J*. 2006;55:2391–2400.
13. Passalacqua A, Marmo L. An explicit method for the packing limit management in dense gas–solid flow CFD simulations on both structured and unstructured grids. *Int J Chem Reactor Eng*. 2007;5:S2.
14. Davidson JF, Harrison D. *Fluidized Particles*. London: Cambridge University Press, 1963.
15. Ellenberger J, Krishna R. A unified approach to the scale-up of gas–solid fluidized bed and gas–liquid bubble column reactors. *Chem Eng Sci*. 1994;49:5391–5411.
16. Geldart D, Radtke AL. The effect of particle properties on the behaviour of equilibrium cracking catalyst in standpipe flows. *Powder Technol*. 1986;47:157–165.
17. Andreux R, Chaouki J. Behaviors of the bubble, cloud and emulsion phases in a fluidized bed. *AIChE J*. 2008;54:406–414.
18. Schiller L, Nauman A. A drag coefficient correlation. *VDI Zeitung*. 1935;77:318–320.
19. Srivastava A, Zenz FA. *Standpipe flow, bubbling aeration and catalyst characterization*. In: *Proceedings of the 5th Annual Fluid Cat Cracking Symposium*. Vienna, Austria: pub. by Katalistiks, Amsterdam, The Netherlands, May 1984: 23–24.
20. Srivastava A, Agrawal K, Sundaresan S, Reddy Karri SB, Knowlton TM. Dynamics of gas-particle flow in circulating fluidized beds. *Powder Technol*. 1998;100:173–182.
21. Karri RBR, Knowlton TM. The effect of aeration on the operation of cyclone diplegs fitted with trickle valves. *I & EC Res*. 2004;48:5783–5789.
22. Knowlton TM, Karri RSB. Differences in cyclone operation at low and high solids loading. In: A. Luckos and P. Smit. *Johannesburg: South African Institute of Mining and Metallurgy*. (Ed.). Industrial Fluidization South Africa 2008;119–160.
23. Jones PJ, Leung JS. Downflow of solids through pipes and valves. In: Davidson J.F., Clift R. and Harrisson D. (eds.). *Fluidization*. London: Academic Press, 1985: 293–327.
24. Zenz FA. Standpipe flow, bubbling aeration and catalyst characterization. In: Proceedings of the 5th Annual Fluid Cat Cracking Symposium, Vienna, Austria, pub. by Katalistiks, Amsterdam, The Netherlands, May 23–24, 1984.
25. Knowlton TM. Standpipe types and modes operation. In: *Proceedings of the 4th SCEJ Symposium on Fluidization*, Sapporo, Japan, 1998: 29–42.
26. Fletcher R. Three-step procedure optimizes FCC slide-valve differential pressure. *Catal Courier*. 1997;30:5–8.
27. Thomas DG. Transport characteristics of suspension. VIII. A note on the viscosity of Newtonian suspensions of uniform spherical particles. *J Colloid Sci*. 1965;20:267–277.
28. Johnson PC, Jackson R. Frictional–collisional constitutive relations for granular materials, with application to plane shearing, *J Fluid Mech*. 1987;176:67–93.
29. Venderbosch RH, Prins W, Kiel JHA, Swaaij WPM. Solids hold-up and pressure gradient in a small laboratory riser. In: Kwauk M, Li J, editors. *Proceedings of the 5th International Conference on Circulating Fluidized Beds*. Beijing, China: Science Press, 1996; pp. 96–102.
30. Konno H, Saito S. Pneumatic conveying of solids through straight pipes. *J Chem Eng Jpn*. 1969;2:211–217.
31. Capes CE, Nakamura K. Vertical pneumatic conveying—an experimental study with particles in the intermediate and turbulent flow regimes. *Can J Chem Eng*. 1973;51:31–38.
32. Yang WC. A correlation for solid friction factor in vertical pneumatic conveying lines. *AIChE J*. 1978;24:548–551.

Manuscript received Apr. 15, 2008, and revision received July 7, 2009.